

Date of publication xxxx 00, 0000, date of current version xxxx 00, 0000.

Digital Object Identifier 10.1109/ACCESS.2017.Doi Number

Enabling Aggregation of Heterogenous Grid-Forming Inverters via Enclaved Homogenization

Muhammad F. Umar, Student Member, IEEE, Mohsen Hosseinzadehtaher, Student Member, IEEE, Mohammad B. Shadmand, Senior Member, IEEE

Intelligent Power Electronics at Grid Edge (IPEG) Research Laboratory Department of Electrical & Computer Engineering, University of Illinois Chicago, IL, USA Corresponding author: Mohammad B. Shadmand (e-mail: shadmand@uic.edu).

This publication was made possible by grant ECCS-2114442 from the U.S. National Science Foundation. The statements made herein are solely the responsibility of the author.

ABSTRACT This paper proposes a control scheme to force homogeneity for heterogenous network of the grid-forming (GFM) inverters in power electronics dominated grid (PEDG) to enable their aggregation and coherent dynamic interaction. Increased penetration of the renewable energy in distributed generation (DG) fashion is moving traditional power system to a highly disperse and complex heterogenous system i.e., PEDG with fleet of grid-forming and grid-following inverters. Optimal coordination, stability assessment, and situational awareness of PEDG is challenging due to numerous heterogenous inverters operating at the grid-edge that is outside the traditional utility centric power generation boundaries. Aggregation of these inverters will not be insightful due to their heterogenous characteristics. The proposed control scheme to force enclaved homogeneity (FEH) enables an insightful aggregation of GFM that can fully mimic the given physical system dynamics. The proposed FEH scheme enables coherent and homogenized dynamic interaction of GFM inverters that enhances the PEDG resiliency. Moreover, different cluster of GFM can be merged into single cluster with minimal synchronization time and frequency fluctuations. Accurate reference models can be achieved that enables effective dynamic assessment and optimal coordination which results in resilient PEDG. Several case studies provided to validate the effectiveness of proposed FEH in network of GFM. Then, GFMs aggregation and developed reference model for the PEDG system is validated via multiple comparative case studies.

INDEX TERMS heterogenous inverter, aggregation, homogenous grid-forming inverters, aggregate reference models

NOMENCLATURE

Agg_{CM}	Aggregated Circuit Model	GFL	Grid-Following inverter
		PCC	Point of Common Coupling
Agg_{MM}	Aggregated Circuit Model	PEDG	Power Electronics Dominate Grid
CB	Circuit Breaker	FEDG	
DG	Distributed Generation	PSC	Power Synchronization
		ROCOF	Rate of Change of Frequency
DER	Distributed Energy Resources		• • •
FEH	Forced Enclaved Homogenization	VSG	Virtual Synchronization Generator
GFM	Grid-Forming Inverter		

I. INTRODUCTION

The traditional power system is under a rapid transition from centrally concentrated generation towards distributed generation (DG) to integrate renewable and sustainable energy such as solar PV, windfarms, etc. with the grid. This integration requires a power electronics interface to regulate and match the dispatchable power according to the grid codes and standards. In most cases an inverter is acting as power electronics interface, and this leads to exponential

growth of inverter based DGs in modern-day grid. Therefore, this leads to a new paradigm known as power electronics dominated grid (PEDG) [1]. PEDG facilitating the integration of renewable energy generation and brings flexibility in the generation mix. The complexity in PEDG is introduced due to its sparse and distributive nature [2, 3]. This complicates the numerical studies on PEDG by increasing the computational burden. Moreover, optimal

Crid Following Inventor

1



coordination [4], stability assessment [5] and situational awareness in PEDG becomes a challenging task.

An insightful aggregated model which preserves the large and interconnected power system's dynamic and steady-state response is critical for the PEDG. Nevertheless, accuracy of the developed aggregate model is heavily dependent on the homogeneity of DGs in terms of power ratings, types of controllers, controller gains, filter parameters, etc. Moreover, due to sparseness of generation sources in PEDG, the DGs are not naturally homogenous. Singular perturbation has been widely used to achieve model-order reduction and generate aggregated model of inverters. In this methodology only those states of the model are selected that contributes heavily for the dynamic response of the model and these states are called fast converging states. While slow converging or states that doesn't have much contribution in the dynamic response are ignored. The authors in [6] develop 5th reduced-order model of a grid-forming (GFM) inverter by using singular perturbation method. Moreover, 3rd order, and 1st order model are also deduced but this approach cannot be extended to network level with sufficient accuracy. Another approach proposed in [7] to improve 3rd order model of the droop-based DG. Although, the derived model reports higher accuracy but in the system of inverters such a PEDG this scheme cannot capture all dynamics of system and it considers only fast operating states and ignores the slow dynamics.

Coherency-based aggregation schemes are derived by evaluating swing equation of generating sources. The coherent generation sources are those that have similar dynamics in voltage angle or frequency of the system in the response of a disturbance [8, 9]. Then, by leveraging appropriate model reduction scheme, the grid cluster is aggregated [10]. The initial work on the coherency based model reduction and aggregation of synchronous generators was reported in 1980s and 1990s [11, 12]. The coherencybased aggregation methodologies aids in performing extensive analysis such as optimization of large-scale network and economic dispatch. This is because the coherency-based aggregation schemes preserve majority of the states of the given grid cluster and can truthfully reproduce the dynamic and steady-state response of the large-scale power system.

Generally, the coherency identification schemes can be classified as; (a) model-based schemes [13, 14], and (b) signal-based schemes [15, 16]. In the model-based schemes analysis is performed on the actual mathematical model of the given system to find the coherent sources and then using a model reduction scheme the aggregated model of the given system is derived. For instance, in [17] the authors performs eigenvalue analysis on the model of the cluster under study to find the coherent generation sources. Then, based on this information from the model, the large-order cluster is divided into smaller clusters. The accuracy of the aggregated model derived from the sub-clusters is

highly dependent on the precise and consistent information of the system parameters. However, at many instances full information of the model parameters of the given grid cluster is not available. [18] utilizes a DYNRED software to find the slow coherency of the synchronous generators in the grid cluster under study. Nevertheless, the proposed scheme is limited to specific equilibrium points and general analysis is not possible. Moreover, it suffers from the parametric uncertainties and imperfections in the modeling. On contrary, the signal-based scheme utilizes the wide-area monitoring for instance synchrophasors. These signals are then used to obtain useful from the system under study. [13] proposed a scheme that determines the coherent generators and partition into electrical area from a large, interconnected power system. This scheme is based on dynamic frequency deviations from generator and nongenerator buses with respect to the nominal frequency of the given system. The advantages of using the schemes based on signal measurement are fast and dynamic identification of coherency and low dependence on the data from the model [19]. But, due to external disturbances the information received via a wide area monitoring device have reliability issues.

Originally, the coherency-based aggregation schemes are utilized to derive the reduced-order models for the cluster of interconnected generators. However, these concepts of coherency can be extended to made applicable for the DGs. Broadly, depending on the implemented control and interaction with the grid the DGs can be classified as grid forming (GFM) inverter-based DGs and grid following (GFL) inverter-based DGs. The primary goal in the control of GFM inverter is to regulate the voltage and frequency of the system. Prevailing from more than two decades droop-based control for GFM has been most mature and widely known scheme [20]. Concepts of droopbased control initiates from the governor action which allow the parallel operation of the multiple DGs. Initially, the frequency based droop control has been proposed in [21] for the islanded AC and uninterruptible power supplies. The improved transient response of the classical frequency-droop control was proposed in [22]. This improvement was proposed by incorporating the integral and a derivative term in the active power path. Power synchronization control (PSC) is another method for controlling the GFM inverters. PSC has a similar controller structure to droop control structure. Instead of frequency variation the voltage angle is drooped in response to variation in the power. The work in [23] proposes a PSC for a HVDC system which improves the converter dynamics operating in the weak grid conditions. Furthermore, the control of GFM can mimic a synchronous machine by utilizing a swing equation. This type of control is commonly known as virtual synchronous generator (VSG) [24]. The concept of VSG is proposed in [25] which is based on the swing equation of the synchronous generator. In [26], a comparison between the dynamics of VSG and droop-based control is presented. It has been concluded that



a droop-based control with a low-pass filter is mathematically equal to the VSG. Moreover, a droop control low pass filter can mimic the virtual inertia offered by the VSG and it is the special case of VSG. A comprehensive analysis on the control strategies reported in literature for the distributed generation under various operating conditions is presented in [27]. The comparative assessment on various grid-forming scheme is given in [28]. A missing piece of puzzle in these existing works is the detailed dynamic interaction analysis of the commonly heterogeneous GFM inverters. Furthermore, the accurate aggregation of these inherently heterogenous GFM inverters is not well studied in literature. This paper is addressing these two research gaps by a tertiary control layer for developing force enclaved homogenization (FEH) of network of GFM inverters which enables coherent dynamic response to disturbances. Furthermore, the proposed FEH scheme enables an accurate aggregation of GFM inverters.

Specifically, the GFM inverters based DGs can be called coherent if these have identical voltage angle and frequency response to a disturbance. Moreover, these can be clustered into a single and unified model. For instance, [29] utilizes the concepts of differential geometry to find the coherency among the system of interconnected DGs. But application of the proposed methodology on large-order system is complex and requires extensive analysis and validation. [30] presents a structure preserving scheme for aggregating three parallel connected inverters and represents the inverters as single and unified model. However, with different filter parameters and locally generated control gains for each inverter it is hard to achieve a lumped system. [31] proposes model aggregation scheme for the interconnected GFM inverter based DGs. Singular perturbation method is utilized to aggregate the system. However, this work only considers DGs that are initially coherent and partition that into study area and all other network as external area and lumped by using Kron reduction. A coherency enforcement scheme introduced in [32] based on virtual impedance for the GFM inverters. Eigenvalue perturbation scheme is applied to find the extinct of coherency among the droop controller GFM inverter. Nevertheless, the proposed scheme only considered the dynamics of the droop-based inverters and ignored the dynamics of the interconnected system. Moreover, the parameters of each inverter are considered homogenous which is practically rare.

A coherency-based aggregation scheme is proposed in this paper. Specifically, the concepts of coherency are applied on PEDG with heterogenous GFM inverters. Thus, with the proposed scheme a forced enclave homogenization (FEH) of the GFM is achieved. The requirement for the forced enclave homogenization among the GFM inverter based DGs is that if voltage angle or frequency of the DGs responds in similar manner to the external disturbance then that group of DGs are considered enclaved homogenized.

This work considers each GFM inverter with heterogenous parameters such as, power ratings, filter parameters, types of controller and controller gains. Thus, this work encompasses more practical system which includes inherently heterogenous DGs that will not have similar dynamic response and cannot be enclaved. Therefore, the FEH is devised that is based on autonomously obtaining the equivalent inertia of the given network of DGs. Then, devising the controller gains and this force enclaved homogenization in the PEDG. Furthermore, the dynamic model of the GFM inverter is developed and then based on this model the aggregate reference model for the forced enclave homogenized DGs is devised. The accuracy of the devised aggregate model is validated by comparing its dynamic and steady-state response under a disturbance with the circuit model of individual DGs and aggregated DGs. Furthermore, the proposed FEH scheme was tested under the cluster reconfiguration. Specifically, the case study for the cluster merging was performed when two cluster having different number of DGs are merged. The supervisory layer adjusts the controller parameter in real-time to restore the coherency among the new merged cluster. Comparatively, with the proposed scheme the synchronization time for clustering was greatly reduced without noticeable frequency and voltage fluctuations.

The structure of the remainder of the paper is: section II explains the development of FEH via equivalent inertia emulation. Section III formulates the model of GFM inverter for dynamical analysis and aggregate reference model. The validation of the proposed scheme is explained in section IV. Finally, the paper is concluded in section V.

II. PROPOSED FORCE ENCLAVED HOMOGENIZATION CONTROL

A. FORMULATION OF FEH CONTROL

The structure of the proposed FEH control scheme for the GFM inverters in PEDG is illustrated in Fig. 1. In the PEDG, the conventional active and reactive power droop control relations will no longer be fully decoupled and are given by,

$$f - f_0 = m_p (P_{nom} - P_f) + n_q (Q_f - Q_{nom})$$
 (1)

$$v - v_0 = m_p (P_{nom} - P_f) - n_a (Q_f - Q_{nom})$$
 (2)

where $m_p = k_p(X/Z)$, $n_q = k_q(R/Z)$ are the effective frequency and voltage droop gains, respectively. These effective droop gains are dependent on the ratios of resistive and inductive line impedances between the two power sharing grid-forming inverters. P_{nom} and Q_{nom} refers to the nominal active and reactive power. $P_f = P_{me}(\omega_c/(s+\omega_c))$, $Q_f = Q_{me}(\omega_c/(s+\omega_c))$ is the determined active power and reactive power after filtering via low-pass filter. The nominal frequency and voltage are denoted by f_0 and v_o ; ω_c is the cutoff frequency of the low-pass filter.



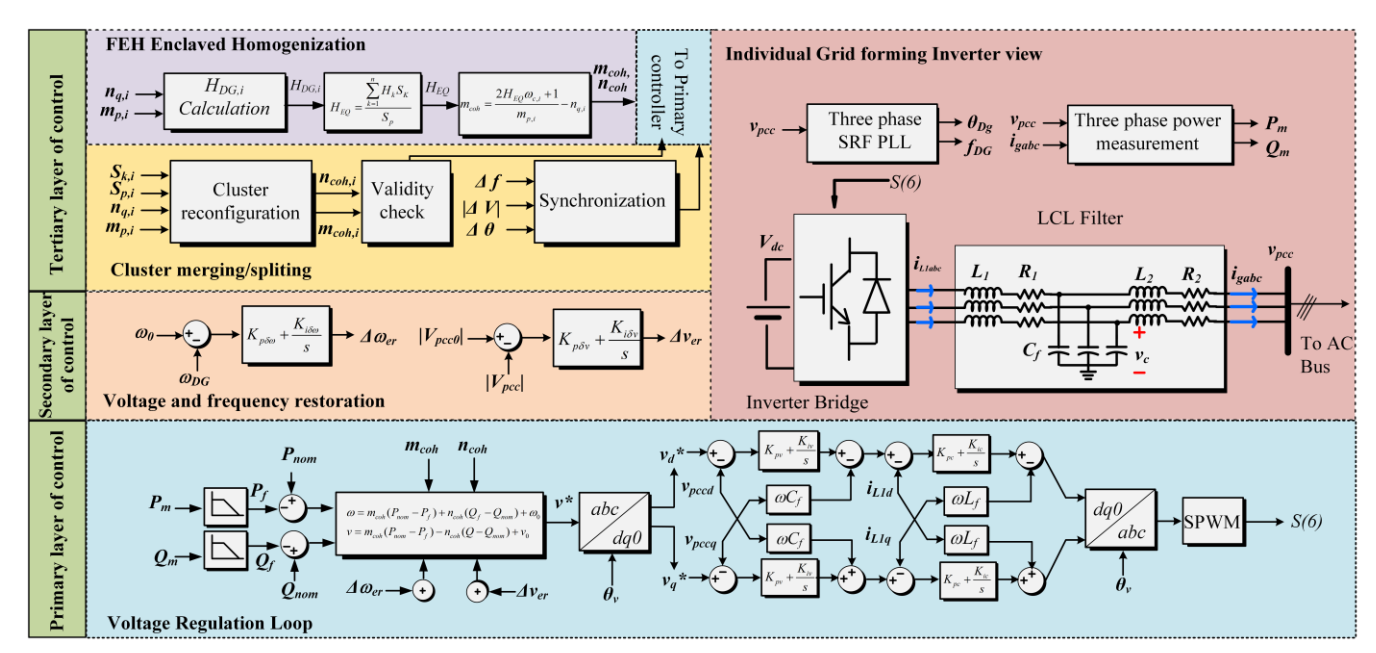


Figure 1. Proposed force enclaved homogeneity (FEH) controller structure

The virtual inertia emulation from the grid-forming inverter is formulated by leveraging the swing equation of synchronous generator. Considering the frequency deviations are small around the nominal frequency and active and reactive power set-points are fixed. The modified swing equation for the grid-forming inverter given in per unit as,

$$4\pi f H \frac{df}{dt} = P_{nom} - P + D_p(f - f_0)$$
(3)

$$f - f_0 = \frac{2sH\omega + P - P_{nom}}{D_p} \tag{4}$$

where, inertia constant is denoted by H, damping coefficient as D_p , and f is termed as rate of change of frequency (ROCOF). By evaluating (4) and (1) an equivalence can be derived between the active power droop equation and the swing equation. Therefore, after equating (4) and (1) and assuming steady-state conditions such as the nominal active and reactive power is supplied by the inverter. Then relation between H and m_p is given by,

$$m_{p,i+1} = \frac{2H\omega_c + 1}{m_{p,i}} - n_{q,i}; \ m_{p,i}D_{p,i} = 1$$
 (5)

To derive the equivalent inertia constant of whole PEDG comprising *n* number of DGs, firstly inertia constant for each DG is calculated by solving (5) via iterative process. Then, based on each DG's rated or nominal power and calculated inertia constants, the equivalent inertia of the PEDG is given as,

$$H_{EQ} = \frac{\sum_{k=1}^{n} H_k S_K}{S_p}$$
 (6)

where, H_{EQ} is denoted by equivalent inertia of the grid cluster under consideration, H_k is each DG's individual inertia constant, S_k , S_p are the rated apparent power of i_{th} DG. Therefore, the droop coefficients required to force enclaved homogenization among the DGs in PEDG is given by,

$$m_{coh(1,2,\dots,n)} = \frac{2H_{EQ}\omega_{c,i} + 1}{m_{p,i}} - n_{q,i}$$
 (7)

Furthermore, the upper limit on the coherent droop coefficients is devised based on the standard EN 50438 [33] and are given as,

$$m_{\max,i} = \frac{\Delta \omega_{\max}}{\Delta P_{\max}} = \frac{2\% \omega_0}{100\% P_0}$$

$$n_{\max,i} = \frac{\Delta V_{pcc-\max}}{\Delta Q_{\max}} = \frac{10\% V_{pcc0}}{100\% Q_0}$$
(8)

The proposed FEH scheme is based on the calculation of the equivalent inertia constant H_{EO} of the cluster by leveraging the control parameters. The supervisory control layer receives the information by communicating with primary controllers of each DG. Based on each DGs droop parameters, the virtual inertia emulated by each DG is calculated in (5). Moreover, the equivalent inertia of the cluster is calculated by (6). Then, based on this equivalent inertia of the cluster, the droop coefficients that will enforce homogeneity among the heterogenous DG are devised in the supervisory layer. Next in the supervisory layer of control the modified droop gains are checked for compliance of the standard EN 50438 [33]. This modified droop gains are communicated to the primary controllers of the DGs to incorporate them in the control loop in realtime.



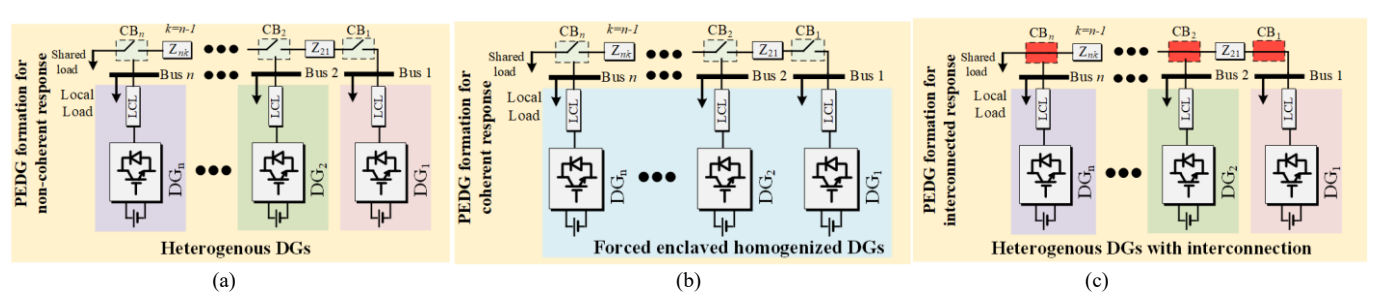


Figure 2. System configuration in the cluster of *n* DGs: (a) heterogenous DGs without interconnection, (b) force enclave homogenized DGs without interconnection, (c) heterogenous DGs with interconnection

B. VALIDATION OF PROPOSED FEH IN THE PEDG

This subsection provides validation of the derived mathematical model of the FEH control loop in previous section for a grid cluster comprises of five GFM inverter. Fig. 2 illustrates the system configuration of the cluster under three scenarios; (a) heterogenous DGs without interconnection, (b) forced enclave homogenized DGs without the interconnection, and (c) heterogenous DGs with interconnection. The goal of these case studies is to depict the level of coherency among the heterogenous DGs with the proposed control. The DGs are considered non-coherent and cannot be enclaved in homogenized manner. This is because the GFM inverters have different controller gains, power ratings, and size of filter's components (see Fig. 2(a) and Table I). Moreover, with the proposed control these non-coherent DGs are made coherent and then results are compared with the frequency response derived from the heterogenous DGs with interconnection. Specifically, at instant t_1 the 20kW load step is added. Fig. 3(a) illustrates the frequency response of five heterogenous DGs without the proposed control. Basically, all the DGs exhibits different dynamic frequency response due to heterogenous parameters as given in Table I. However, with the proposed control the heterogenous DGs with different parameters, the dynamic frequency resposne of the DGs is similar or in other words these heterogenous DGs are forced to enclave homogenization, thus these depict coherent dynamic behaviour. Fig. 3(b) confirms this dynamic frequency response of all five DGs. After the 20kW load disturbance at instant t_1 the frequency of the DGs responds in similar manner to the disturbance Fig. 3(b) confirms this dynamic frequency response of all five DGs. After the 20kW load disturbance at instant t_1 the frequency of the DGs responds in similar manner to the disturbance. Moreover, this frequency dynamic response with the proposed control is compared with the frequency dynamic from the heterogenous DGs with response interconnection (see Fig. 2(c) and Fig. 3(c)). By comparing the Fig. 3(b) and Fig. 3(c) it is proven that with proposed control the settling down frequency after the load disturbance is similar to heterogenous DGs with the interconnection. Fig. 3(d) illustrates the shared active power from five DGs in response to the 20kW step increase in load. At instant t₁, the supplied active power from each DG is increased to cater the total 20kW load increase. This

verifies the effective operation of the proposed FEH control under load step without losing the coherent dynamic frequency response.

Furthermore, an additional case study was presented to validate the proposed FEH scheme for achieveing enclaved homogenization. At instant t_2 , a step decrease of 20kW of

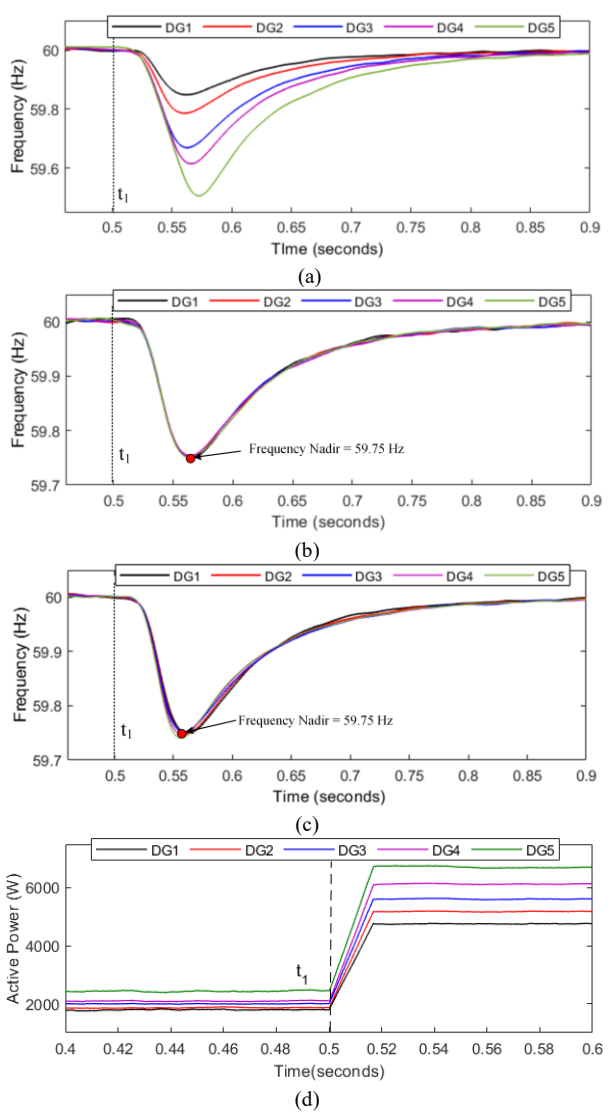


Figure 3. Dynamic response in frequency of DGs in PEDG with load increase: (a) without proposed control (b) with proposed FEH, (c) interconnected PEDG (d) active power profile with proposed FEH



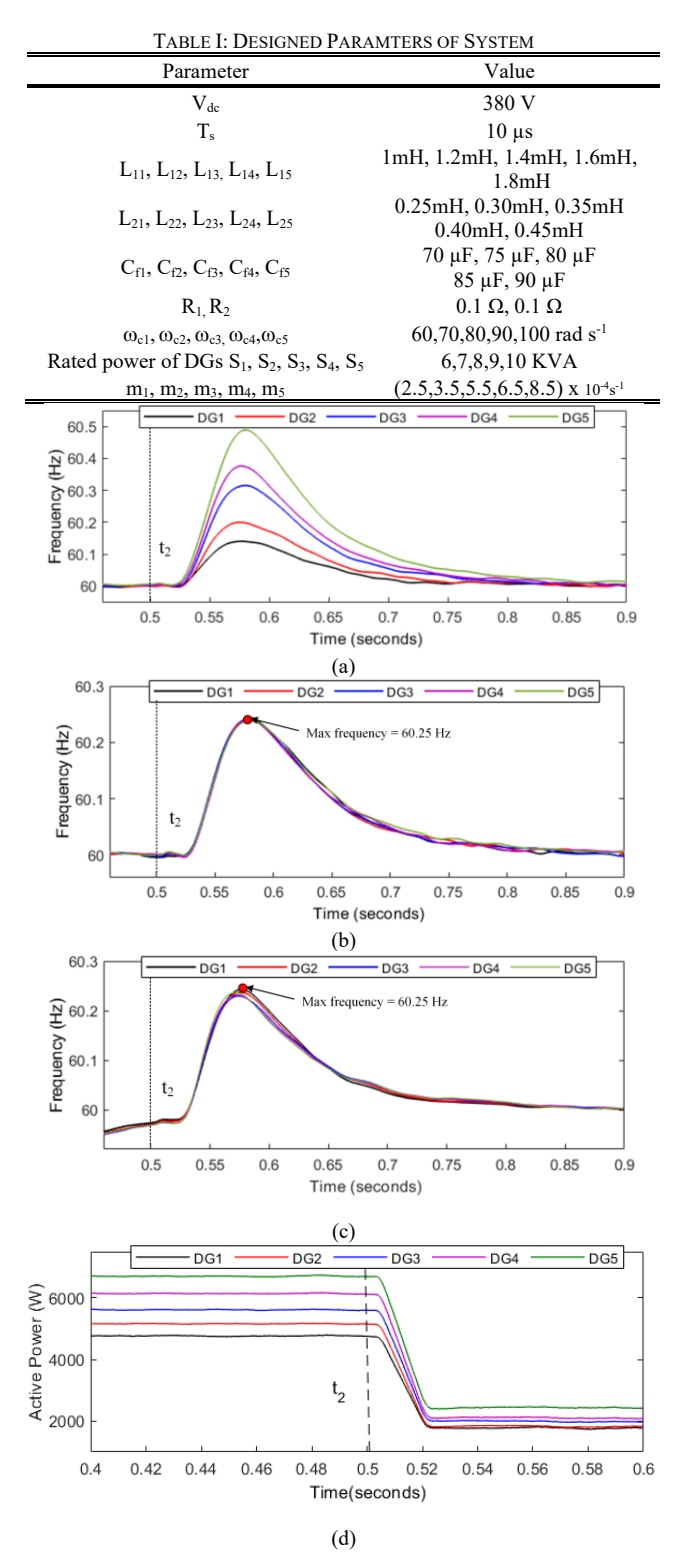


Figure 4. Dynamic response in frequency of DGs in PEDG with load decrease: (a) without proposed control (b) with proposed FEH, (c) interconnected PEDG (d) active power profile with proposed FEH

load is introduced and effect on the frequency dynamic response was observed. Fig. 4(a) illustrates frequency dynamic response of the heterogenous DGs without the proposed control. It can be seen on Fig. 4(a) that each DG

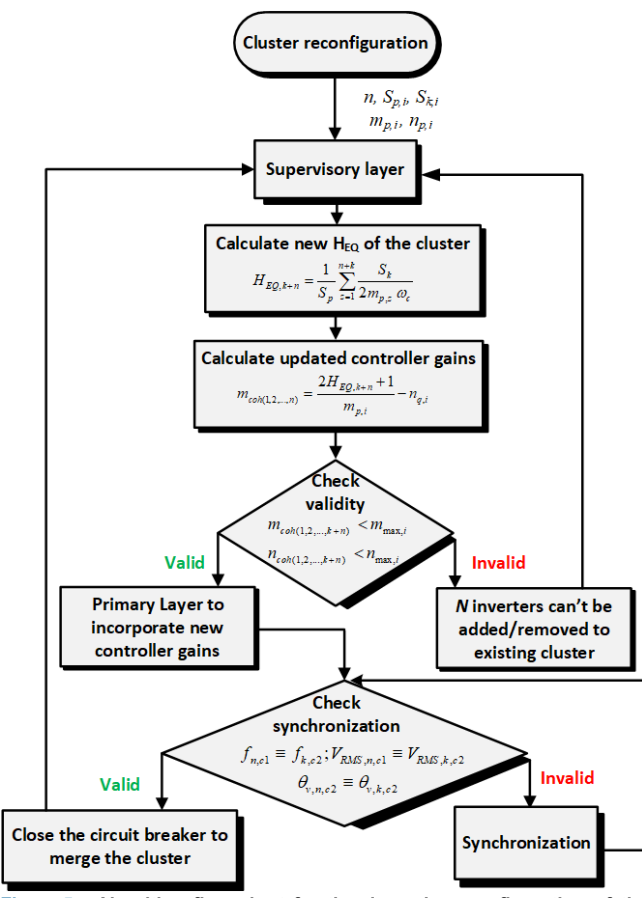


Figure 5. Algorithm flow chart for the dynamic reconfiguration of the cluster via proposed FEH

have non-similar dynamic response in frequency. The Fig. 4(b) depicts the frequency dynamic response of the DG with heterogenous paramters with the proposed control. It is verified that with the proposed control scheme, all the DGs shows similar and coherent frequency dynamic response after the disturbance was introduced at instant t_2 . Moreover, the frequency dynamic response of DGs with proposed control is contrasted against the dynamic response with interconnected DGs as shown in Fig. 4(c). The frequency dynamic response with proposed control matches the dynamic response obtained by making an interconnection in DGs. Moreover after instant t_2 , with the FEH the max frequency reaches to 60.25 Hz while from interconnected DGs the recorded max frequency is 60.25 Hz. Thus, it is verifed that the dynamic response of the five DGs with proposed FEH is similar to the heterogeneous DGs with an interconnection. Fig. 4(d) illustrates the active power profile of five DGs in response to 20kW decremented step change in load. Specifically at instant t₂, the supplied active power share from each DG to the load was decreased with the reduction in load. Similarly, under the load reduction the proposed FEH doesn't collapse from the adverse dynamic interaction of DGs during a disturbance.

Thus, it is proven that in both scenarios, initially heterogenous DGs are forced enclave homogenization and are considered coherent with the proposed control scheme



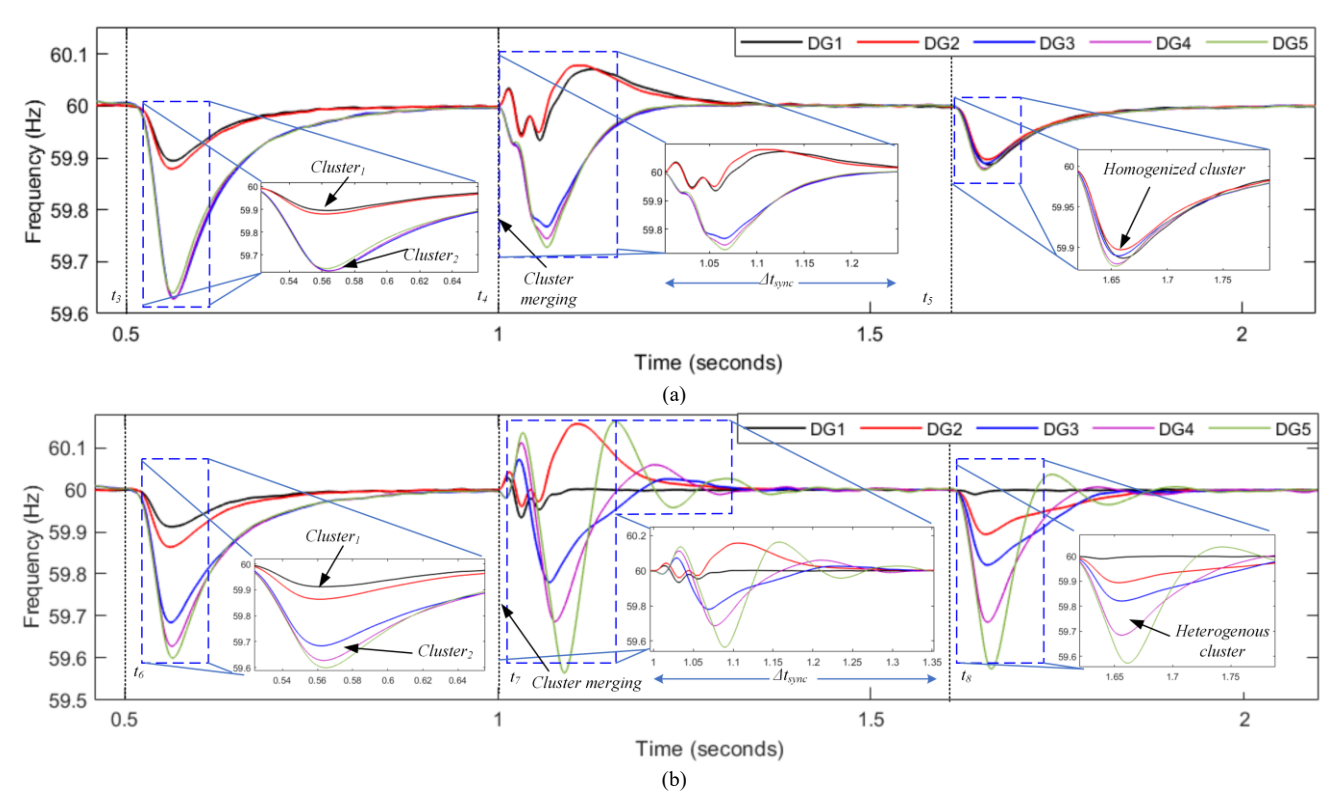


Figure 6. Dynamic frequency response for the reconfiguration of the cluster: merging of two clusters (a) forced enclave homogenized DGs with proposed FEH control (b) heterogenous DGs without the proposed control.

and can be used to derive a unified and aggregate reference model.

C. RECONFIGURATION OF THE CLUSTERS WITH PROPOSED FEH IN THE PEDG

After validating the proposed FEH in the cluster of five GFMs. The effectiveness of proposed FEH for establishing the homogenization in the cluster of heterogenous GFMs is studied under the merging of two clusters. The cluster 1 comprises DG₁ and DG₂ while the cluster 2 consists of DG₃, DG₄ and DG₅. Fig. 5 illustrates the algorithm flow chart for seamless merging two clusters. Specifically, the supervisory level of control is responsible for seamless merging the two clusters. The supervisory layer recieves the information such as the rated power of each DG, rated power of the cluster, and controller gains of the clusters that are required to be merged together. Then, based on the new configuration the equivalent inertia (H_{EO}) of the new cluster is calculated by (6) and then based on this new H_{EO} the droop gains required for forcing enclaved homogenization in the new cluster is devised by (7). Furthermore, a realtime validation mechanism is applied to verfiv the new droop gains are consistent with the standards. If the updated droop gains passes this validation checkpoint then these gains are passed to the primary level controller to incorporate the updated droop gains, otherwise, a signal is generated that clusters cannot be merged to form a new cluster. Furthermore, the synchronization block in the supervisory layer of control ensures the two clusters are

synchronized in terms of frequency, voltage angle and RMS value of the PCC voltage.

Fig. 6 (a) depicts the dynamic frequency response of two clusters with proposed FEH under the event of merging. At instant t_3 , a load disturbance is applied and the frequency responses of two clusters are shown at this instant. DG₁ and DG₂ represents cluster 1 and DG₃, DG₄, and DG₅ denotes the cluster 2. The signal for the cluster merging is generated at instant t_4 . Thus, the updated droop gains are calculated and incorporated in the control. The frequency of DGs tends to deviate from the 60Hz reference, however, due to FEH control a clear improvement in the restoration and synchronization of cluster is shown. Significantly, the time required for frequency restoration and synchronization during the cluster merging is mere 0.20 seconds. Furthermore, at instant t_5 a load disturbance is applied to verify that merged cluster is showing homogenized frequency response. Thus, it can be verifed from the dynamic frequency response at instant t_5 that new cluster is behaving as a single cluster and the two clusters are safely merged together.

Fig. 6 (b) illustrates the dynamic frequency response with heterogenous DGs under the event of merging. A load disturbance is applied at instant t_6 and it can be seen that cluster 1 and cluster 2 shows the different frequency response. At instant t_7 the signal for merging of two clusters is given to the supervisory layer of control. As the DGs have heterogenous paramters and characteristics, thus a large frequency deviation is depicted at instant t_7 . More importantly the time required for the cluster



synchronization and frequency restoration exceeds 0.5 seconds and cluster was merged at time equals to 1.55 seconds. It can be seen that during cluster merging the DGs were facing very high ROCOF and frequency deviations due to adverse dynamic interactions between the two cluster. Moreover, at instant t_8 a load disturbance was introduced to validate the merging of cluster and it can be verified as the load disturbance was applied the DGs are behaving as a single cluster with herterogenos frequneyc response.

III. AGGREGATION OF GRID-FORMING INVERTER WITH THE PROPOSED FEH

A. DYNAMIC MODEL OF A SINGLE GRID-FORMING INVERTER WITH FEH CONTROL LOOP

After establishing the coherent frequency dynamic response in the given PEDG, the dynamic model of a single GFM is developed. This model acts as a groundwork for aggregation of grid cluster with multiple GFMs. The full order model of the GFM comprises of fourteen states. The dynamics equations of active and reactive power and voltage angle are given by,

$$\omega = \omega_0 - m_n (P_f - P_{nom}) \tag{9}$$

$$\theta = \omega_0 t - m_n \int (P_f - P_{norm}) dt \tag{10}$$

$$V_{nccd}^* = V_{nccd} - n(Q_f - Q_{nom})$$
 (11)

$$V_{pcca}^* = 0 (12)$$

Furthermore, the state-space model is developed by linearzing and rearranging (9)-(12) and is given by,

$$\begin{bmatrix} \theta \\ P \\ Q \end{bmatrix} = A_1 \begin{bmatrix} \theta \\ P \\ Q \end{bmatrix} + B_1 \begin{bmatrix} i_{1dq} \\ V_{pccdq} \\ i_{gdq} \end{bmatrix} + B_2 [\omega_c]$$

$$\begin{bmatrix} \omega \\ V_{pcc-dq} \\ Q \end{bmatrix} = C_1 \begin{bmatrix} \theta \\ P \\ Q \end{bmatrix} + D_1 \begin{bmatrix} i_{1dq} \\ V_{pccdq} \\ i_{gdq} \end{bmatrix}$$
(13)

where,

where,
$$A_{1} = \begin{bmatrix} 0 & -m_{coh} & 0 \\ 0 & -\omega_{c} & 0 \\ 0 & 0 & -\omega_{c} \end{bmatrix}$$

$$B_{1} = \begin{bmatrix} 0 & 0 & 0 & 0 & 0 \\ 0 & 0 & 3\omega_{c}i_{gd} & 3\omega_{c}i_{gq} & 3\omega_{c}v_{pccd} & 3\omega_{c}v_{pccq} \\ 0 & 0 & \omega_{c}i_{gq} & \omega_{c}i_{gd} & -\omega_{c}v_{pccq} & -\omega_{c}v_{pccd} \end{bmatrix}, B_{2} = \begin{bmatrix} -1 & 0 & 0 \end{bmatrix}^{T}$$

$$C_{1} = \begin{bmatrix} 0 & -m_{coh} & 0 \end{bmatrix}, C_{2} = \begin{bmatrix} 0 & 0 & -n_{coh} \\ 0 & 0 & 0 \end{bmatrix}$$

$$D_1 = D_2 = 0_{1\times 3}$$

where ω and ω_0 represents the instantaneous frequency and nominal frequency of DGs, respectively. The voltage angle is denoted by θ , the d-q components of the output current is represented as i_{gd} and i_{dq} , d-q component of the PCC voltage is termed by v_{pccd} and v_{pccq} , the droop gains required to make DGs coherent is defined as m_{coh} that is devised by the coherency enforcement control loop.

To capture the dynamics of the converter side voltage, inductor L_1 current, PCC voltage, and output current dynamic equations in d-q reference frame are given by,

$$\frac{di_{1d}}{dt} = -\frac{R_1}{L_1}i_{1d} + \omega i_{1q} + \frac{1}{L_f}(v_{invd} - v_{cd})$$
 (14)

$$\frac{di_{1q}}{dt} = -\frac{R_1}{L_1}i_{1q} + \omega i_{1d} + \frac{1}{L_f}(v_{invq} - v_{cq})$$
 (15)

$$\frac{dv_{cd}}{dt} = \omega v_{cd} + \frac{1}{C_f} (i_{1d} - i_{gd})$$
 (16)

$$\frac{dv_{cq}}{dt} = -\omega v_{cq} + \frac{1}{C_f} (i_{1q} - i_{gq})$$
 (17)

$$\frac{di_{gd}}{dt} = \frac{-R_1 - R_2}{L_1 + L_2} i_{gd} + \omega i_{gq} + \frac{1}{L_1 + L_2} (v_{cd} - v_{pccd})$$
 (18)

$$\frac{di_{gq}}{dt} = \frac{-R_1 - R_2}{L_1 + L_2} i_{gq} - \omega i_{gd} + \frac{1}{L_1 + L_2} (v_{cq} - v_{pccq})$$
(19)

By evaluating the (14)-(19) a state-space model is derived and given as,

$$\begin{bmatrix} i_{1-dq} \\ v_{c-dq} \\ v_{c-dq} \\ i_{g-dq} \end{bmatrix} = A_2 \begin{bmatrix} i_{1-dq} \\ v_{c-dq} \\ i_{g-dq} \end{bmatrix} + B_3 [v_{inv-dq}] + B_4[\theta] + B_5[\omega]$$
(20)

$$[v_{inv-dq}] = C_4[\xi_{dq}] + D_5[i_{1-dq}] + D_6\begin{bmatrix} i_{1-dq} \\ v_{c-dq} \\ i_{g-dq} \end{bmatrix}$$

where

$$A_{2} = \begin{bmatrix} \frac{R_{1}}{L_{1}} & \omega & \frac{-1}{L_{1}} & 0 & 0 & 0 \\ -\omega & \frac{-R_{1}}{L_{1}} & 0 & \frac{-1}{L_{1}} & 0 & 0 \\ \frac{1}{C_{f}} & 0 & 0 & \omega & \frac{-1}{C_{f}} & 0 \\ 0 & \frac{1}{C_{f}} & -\omega & 0 & 0 & \frac{-1}{C_{f}} \\ 0 & 0 & \frac{-1}{L_{1} + L_{2}} & 0 & \frac{-R_{1} - R_{2}}{L_{1} + L_{2}} & \omega \\ 0 & 0 & 0 & \frac{1}{L_{1} + L_{2}} & -\omega & \frac{-R_{1} - R_{2}}{L_{1} + L_{2}} \end{bmatrix}$$

$$B_{4} = \begin{bmatrix} 0 & 0 & 0 & 0 & \frac{v_{pec} \sin \theta_{v}}{L_{1} + L_{2}} & \frac{-v_{pec} \cos \theta_{v}}{L_{1} + L_{2}} \end{bmatrix}^{T}$$

$$B_{5} = \begin{bmatrix} i_{1q0} & -i_{1d0} & v_{cq0} & -v_{cd0} & i_{gq0} & -i_{gd0} \end{bmatrix}^{T}$$

$$C_{4} = \begin{bmatrix} K_{fc} & 0 \\ 0 & K_{rc} \end{bmatrix}$$

$$D_{5} = \begin{bmatrix} K_{pc} & 0 \\ 0 & K_{pc} \end{bmatrix}, D_{6} = \begin{bmatrix} -K_{pc} & -\omega L_{1} & 0 & 0 & 0 \\ \omega L_{1} & -K_{pc} & 0 & 0 & 0 \end{bmatrix}$$



TABLE II: INITIAL CONDITIONS

Parameter	Value
Output current i_{gd0} , i_{gq0}	0.25 A, 0.02 A
Reactive power Q_0	-10 VARs
VPCC angle $\theta_{v\theta}$	0.3 rad/s
Filter capacitor voltage v_{cd0} , v_{cq0}	123 V, 2 V
Converter-side current i_{Id0} , i_{Iq0}	0.74 A, 0.03 A
Point of common coupling voltage v_{pccd0} , v_{pccq0}	122 V, 0 V
Active power P_{θ}	50 W

where, the filter capacitor voltage in d-q reference frame is given as v_{cd} and v_{cq} , K_{pc} , K_{lc} , K_{vc} are the PI controller gains, v_{invd} and v_{inq} are the d-q components of the inverter-side voltage. The calculation of the inverter-side voltage involves the ξ_{dq} that is represented as the controller states in d-q reference frame. The state-space representation for the calculation of the controller states is given as,

$$\begin{bmatrix} \boldsymbol{\xi}_{dq}^{\square} \end{bmatrix} = A_3 \begin{bmatrix} i_{1-dq} \end{bmatrix} + B_6 \begin{vmatrix} i_{1-dq} \\ v_{c-dq} \\ i_{g-dq} \end{vmatrix}$$
 (21)

where,

$$A_3 = \begin{bmatrix} 1 & 0 \\ 0 & 1 \end{bmatrix}, B_6 = \begin{bmatrix} -1 & 0 & 0 & 0 & 0 & 0 \\ 0 & -1 & 0 & 0 & 0 & 0 \end{bmatrix}$$

Furthermore, the initial values of the states of the grid-forming DG given in matrix B_5 is mentioned in Table II.

B. AGGREGATED REFERENCE MODEL OF THE PEDG: A GRID CLUSTER WITH INTERCONNECTED GFM BASED PROPOSED FEH

Based on the dynamical model of grid-forming DG presented in the previous subsection, an aggregated model of PEDG comprising of five GFM inverters is developed. Furthermore, the five inverters are initially heterogenous having the parameters mentioned in the Table I. Then, coherency was enforced via FEH controller. As, the switching frequency is high, thus the equivalent filter parameters for the aggregated reference model are approximated as,

$$\begin{split} L_{1eq} &= L_{11} / / L_{12} ... / / L_{1n} \\ L_{2eq} &= L_{21} / / L_{22} ... / / L_{2n} \\ R_{1eq} &= R_{2eq} = R_{12} / / R_{12} ... / / R_{1n} \\ C_{feq} &= C_{f1} / / C_{f2} ... / / C_{fn} \end{split} \tag{22}$$

Moreover, as the equivalent proportional and integral coefficients K_{pveq} and K_{iveq} of the voltage regulator given as,

$$K_{pveq} = \sum_{n=1}^{n} K_{pvn}$$

$$K_{iveq} = \sum_{n=1}^{n} K_{ivn}$$
(23)

where n refers to the controller number for the grid-forming inverters in the PEDG.

IV. RESULTS AND DISCUSSION

The aggregate reference model is perturbed under a disturbance by changing the load. Two case studies (Fig. 7 and Fig. 8) are presented to validate the proposed approach. To verify the accuracy of the developed aggregate reference model a comparison between the circuit model and mathematical model is presented. In Fig. 7 and Fig. 8, the labels Agg_{CM} and Agg_{MM} represents the aggregate circuit model and aggregate mathematical model signals respectively for each of the presented parameters. The labels DG₁ to DG₅ are the individual DGs circuit-based signals for each of the presented parameters. Additionally, in the case studies various parameters of individual DGs is also presented and discussed. For the aggregated reference model, the initial conditions for the states are given in the Table II.

A. CASE STUDY I: INCREASE IN LOAD

At instant t_3 the load was increased to 66.67% and the effect of this disturbance was observed on the aggregated reference model, aggregated circuit model and individual DGs. Fig. 7(a) illustrates the dynamics in the active power of aggregated reference model, aggregated circuit model and individual DGs. Specifically, before instant t_3 active power injection from aggregate reference model and aggregated circuit model matches to 4.92 kW. Moreover, active power injection from the five individual DGs is adds up to 4.9 kW. After t_3 when 66.67 % load was increased the active power injection from aggregate reference model and aggregated circuit model increases to 14.96 kW in response to the increase in the active power load demand. Furthermore, active power injection from the each individual DGs sums up to 14.91 kW. It is worthy to note that before and after load increase the active power injection from aggregate reference model, aggregated circuit model and composite active power individual DGs is equated with negligible differences.

Fig. 7(b) depicts the impact of the load disturbance on the inductor L_1 current in d-axis of the aggregate reference model, aggregate circuit model and the five individual DGs. Before and after instant t_3 , the inductor L_1 current in d-axis of the aggregate reference model equals inductor L_1 current in d-axis of aggregate circuit model i.e., 19.45 A before instant t_3 and 58.70 A after t_3 . Additionally, the summation of the inductor L_l current in d-axis of each individual DGs before and after disturbance is 19.45 A and 58.70 A, respectively. Thus, this summation of current also matches with the developed aggregate reference model. Fig. 7(c) illustrates the dynamics in the inductor L_1 current in q-axis for the developed aggregate reference model, aggregate circuit model and the five individual DGs. Majorly, a step increase was in active load at instant t_3 , thus the inductor L_1 current in q-axis remain near to the zero. Although there is a small deviation at instant t_3 when load was switching to higher value but again in very minimal time the q-axis current of the aggregate reference model returns to zero with a negligible deviation. Moreover, as seen in the zoom



in windows the developed aggregate reference model and circuit model matches each DG's output.

The output current in d-axis for the aggregate reference model, aggregate circuit model and the five individual DGs is shown in the Fig. 7(d). To cater the step increase in the active power, the output current increases and that is verified in Fig. 7(d). Specifically, at instant t_3 value of output current in d-axis for the aggregate reference model and aggregate circuit model increases from 19.35 A to the 58.60 A. Although the developed aggregate reference model shows a ringing at instant t_3 but that is for very minimal duration and ultimately settles to the value that exactly matches the aggregate circuit model. Moreover, the summation of the output current in d-axis for the five individual DGs matches with the aggregate reference model before and after instant t_3 . Fig. 7(e) and (f) represents the PCC voltage in d-q axis for the aggregate reference model, aggregate circuit model and the five individual DGs. It is verified that at instant t_3 the d-q axis value of the PCC voltage remains stiff at 169 V and 0 V, respectively. Although at instant t_3 , there is a small deviation from the reference values, however, the PCC voltage in d-q axis for the aggregate reference model, aggregate circuit model and five individual DGs returns to the reference value in nominal time.

B. CASE STUDY II: DECREASE IN LOAD

The transients in the aggregate reference model due to the sudden decrement in the load at instant t_4 is presented in this case study. Fig. 8(a) illustrates the decrement in active power injection from the aggregate reference model, aggregate circuit model and five individual DGs. The active power from the aggregate reference model and aggregate circuit model decreases from 14.66 kW to the 4.84 kW. Moreover, the summation of active power injection from five DGs before and after instant t_4 is 14.65 kW to 4.82 kW, respectively. This verifies that developed aggregate reference model matches the active power injection from the aggregate circuit model and as well as summation of active power from five individual DGs.

Fig. 8(b) and (d) illustrates the decrement in the inductor L_1 current and output current in d-axis from the aggregate reference model, aggregate circuit model and five DGs. Significantly, at instant t_4 , the output current in d-axis of the aggregate reference model and aggregate circuit model decreases from 58.51 A to 19.38 A. Moreover, the summation of currents from the five DGs also matches with the developed aggregate reference model. Fig. 8(d) and (f) illustrates the PCC voltage in d-q axis from the aggregate reference model, aggregate circuit model and five individual DGs. Specifically at instant t_4 , the PCC voltage deviates from reference values of 169V and 0V in d-q axis, respectively. However, it can be clearly seen that in a minimal time the voltage restores to the reference values. Therefore, this verifies that dynamic response of the developed aggregate reference model under transients and steady state matches the aggregate circuit model and as well

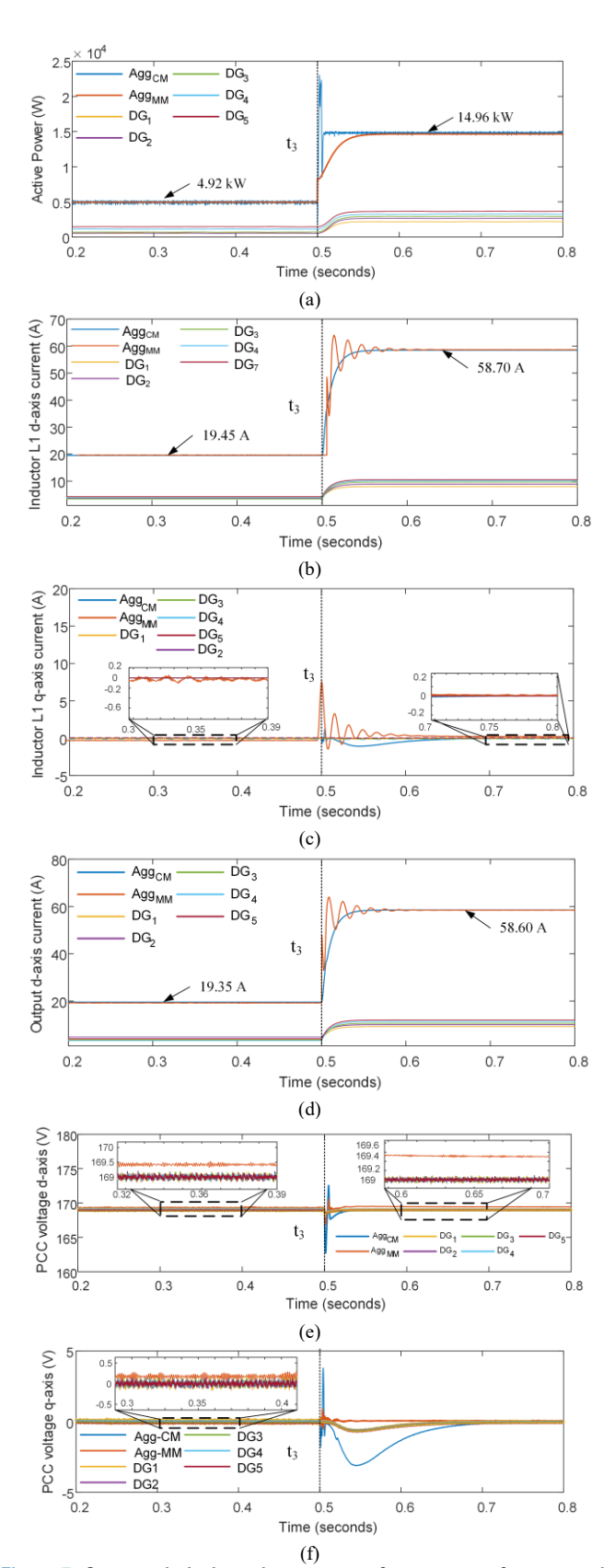


Figure 7. Case study I: dynamic response of aggregate reference model and circuit of PEDG under disturbance of load increase: (a) active powers, (b) inductor L1 d-axis current, (c) inductor L1 q-axis current., (d) output d-axis current., (e) PCC voltage d-axis, (f) PCC voltage q-axis.



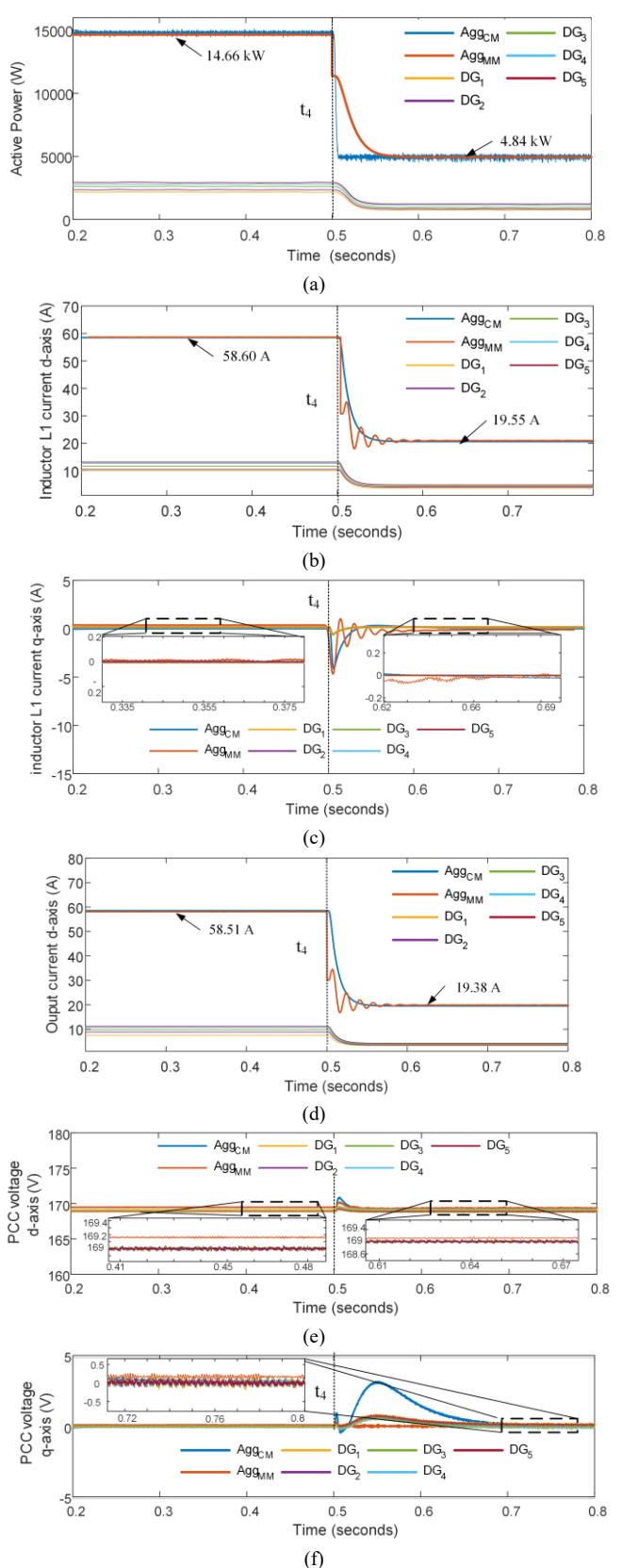


Figure 8. Case study II: dynamic response of aggregate reference model and circuit of PEDG under disturbance of load decrease: (a) active powers, (b) inductor L1 d-axis current, (c) inductor L1 q-axis current., (d) output d-axis current., (e) PCC voltage d-axis, (f) PCC voltage q-axis.

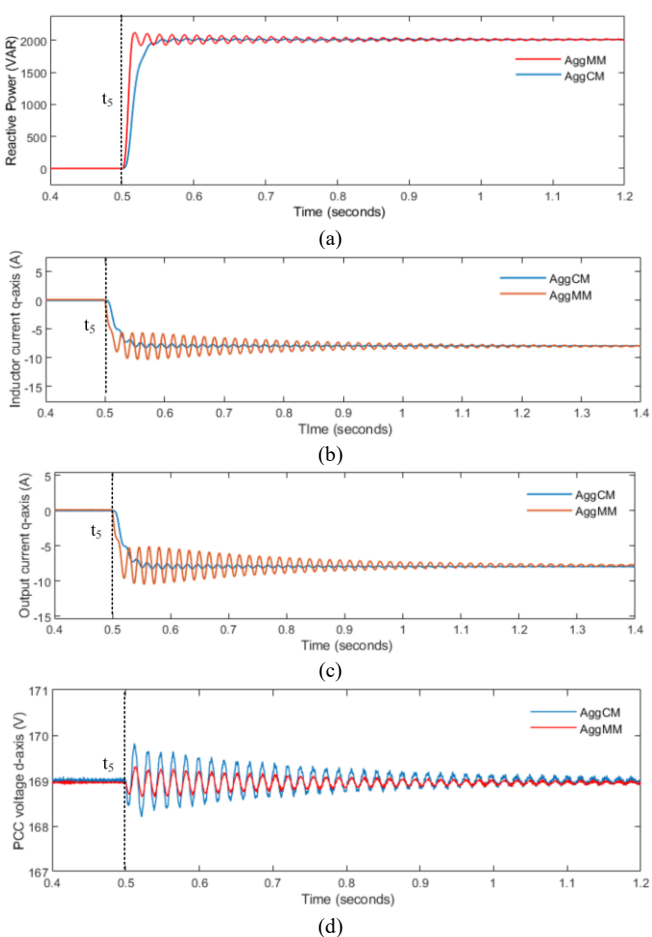


Figure 9. Case study III: dynamic response of aggregate reference model and circuit model of PEDG under step change in reactive power: (a) reactive powers, (b) inductor current L1 q-axis, (c) output current q-axis, (d) PCC voltage d-axis

studies depict the high accuracy of the developed aggregate reference model.

C. CASE STUDY III: REACTIVE POWER SUPPORT

The developed aggregate reference model of cluster of PEDG is tested for the reactive power support after adding a reactive load. One of the primary roles of the GFM inverter is to supply reactive power in case of requirement of reactive power from the grid. Specifically, at instant t_5 a reactive load of 2000 VARs is connected, and effect of reactive load addition was studied on the developed aggregate reference model and compared with the full-scale circuit model of PEDG cluster. Fig. 9 (a) illustrates the reactive power profile of aggregate reference model and circuit model. It can be verified at instant t_5 the reactive power from the aggregate reference model and circuit model increases from 0 to 2000 VARs to supply the reactive load. The developed aggregate model closely matches the circuit model with a small diminishing ripple. Moreover, the inductor L_1 q-axis current from the aggregate reference model and the circuit model depicted in Fig. 9 (b). It changes from 0 to -7.58 A to supply the current to a reactive load. Fig. 9 (c) illustrates the output current from the aggregate reference model and the circuit model that



also changes from 0 to -7.62 A. Although the output from the aggregate reference model has a small ripple but it diminishes within a short duration and proposed control is able to supply the reactive power without any instability. The small diminishing ripple is also present in the output from the circuit model. This is because the controller is trying to regulate demand of reactive power and the system is transitioning. Additionally, the stable operation of the proposed control and the developed aggregate reference model is verified in Fig. 9 (d). The d-axis component of the PCC voltage from the aggregate reference model and circuit model is 169 V with a small negligible ripple and even this ripple dies down at t = 1.2 s. Thus, this case study validates the stable operation and reactive power support of proposed FEH control. Moreover, the developed aggregate reference model closely matches its circuit model under feeding a reactive load.

V. CONCLUSION

This paper presented a coherency-based aggregation scheme for the interconnected system of the grid-forming inverter based DGs. The considered DGs for the study are inherently heterogenous. Then, based on the proposed equivalent virtual inertia emulation, the force enclaved homogenization scheme was established. This FEH enable coherent dynamic response that enables aggregation of GFMs in a grid cluster. The proposed scheme was verified by presenting various case studies for the network of five DGs. Furthermore, insightful aggregate reference model of the five DGs cluster was developed that was based on the dynamic model of GFM inverter based DGs. High accuracy of the developed aggregate reference model was reported as it was compared with the aggregate circuit model and individual model of five DGs. The developed aggregate reference model closely matches the aggregate circuit and each individual DGs circuit model while supplying active and reactive power loads.

REFERENCES

- [1] Q. Peng, Q. Jiang, Y. Yang, T. Liu, H. Wang, and F. Blaabjerg, "On the Stability of Power Electronics-Dominated Systems: Challenges and Potential Solutions," *IEEE Transactions on Industry Applications*, vol. 55, no. 6, pp. 7657-7670, 2019, doi: 10.1109/TIA.2019.2936788.
- [2] Y. Gu, N. Bottrell, and T. C. Green, "Reduced-order models for representing converters in power system studies," *IEEE Transactions on Power Electronics*, vol. 33, no. 4, pp. 3644-3654, 2017.
- [3] A. Muhtadi, D. Pandit, N. Nguyen, and J. Mitra, "Distributed Energy Resources Based Microgrid: Review of Architecture, Control, and Reliability," *IEEE Transactions on Industry Applications*, vol. 57, no. 3, pp. 2223-2235, 2021, doi: 10.1109/TIA.2021.3065329.
- [4] Q. Peng, T. Liu, S. Wang, Y. Qiu, X. Li, and B. Li, "Determination of droop control coefficient of multi-terminal VSC-HVDC with system stability consideration," *IET Renewable Power Generation*, vol. 12, no. 13, pp. 1508-1515, 2018.
- [5] H. Han, X. Hou, J. Yang, J. Wu, M. Su, and J. M. Guerrero, "Review of power sharing control strategies for islanding

- operation of AC microgrids," *IEEE Transactions on Smart Grid*, vol. 7, no. 1, pp. 200-215, 2015.
- [6] L. Luo and S. V. Dhople, "Spatiotemporal model reduction of inverter-based islanded microgrids," *IEEE Transactions on Energy Conversion*, vol. 29, no. 4, pp. 823-832, 2014.
- [7] P. Vorobev, P.-H. Huang, M. Al Hosani, J. L. Kirtley, and K. Turitsyn, "High-fidelity model order reduction for microgrids stability assessment," *IEEE Transactions on Power Systems*, vol. 33, no. 1, pp. 874-887, 2017.
- [8] R. Podmore, "Identification of coherent generators for dynamic equivalents," *IEEE Transactions on Power Apparatus and Systems*, no. 4, pp. 1344-1354, 1978.
- [9] X. Wang, V. Vittal, and G. T. Heydt, "Tracing generator coherency indices using the continuation method: A novel approach," *IEEE Transactions on Power Systems*, vol. 20, no. 3, pp. 1510-1518, 2005.
- [10] G. Rogers, Power system oscillations. Springer Science & Business Media, 2012.
- [11] J. H. Chow, Time-scale modeling of dynamic networks with applications to power systems. Springer, 1982.
- [12] J. H. Chow, R. Galarza, P. Accari, and W. W. Price, "Inertial and slow coherency aggregation algorithms for power system dynamic model reduction," *IEEE Transactions on Power Systems*, vol. 10, no. 2, pp. 680-685, 1995.
- [13] A. M. Khalil and R. Iravani, "A dynamic coherency identification method based on frequency deviation signals," *IEEE Transactions* on *Power Systems*, vol. 31, no. 3, pp. 1779-1787, 2015.
- [14] A. M. Khalil and R. Iravani, "Power system coherency identification under high depth of penetration of wind power," *IEEE Transactions on Power Systems*, vol. 33, no. 5, pp. 5401-5409, 2018.
- [15] B. P. Padhy, S. Srivastava, and N. K. Verma, "A coherency-based approach for signal selection for wide area stabilizing control in power systems," *IEEE Systems Journal*, vol. 7, no. 4, pp. 807-816, 2013.
- [16] M. Jonsson, M. Begovic, and J. Daalder, "A new method suitable for real-time generator coherency determination," *IEEE Transactions on Power Systems*, vol. 19, no. 3, pp. 1473-1482, 2004.
- [17] S. Yusof, G. Rogers, and R. Alden, "Slow coherency based network partitioning including load buses," *IEEE Transactions on Power Systems*, vol. 8, no. 3, pp. 1375-1382, 1993.
- [18] I. Tyuryukanov, M. Popov, M. A. van der Meijden, and V. Terzija, "Slow Coherency Identification and Power System Dynamic Model Reduction by Using Orthogonal Structure of Electromechanical Eigenvectors," *IEEE Transactions on Power Systems*, vol. 36, no. 2, pp. 1482-1492, 2020.
- [19] V. Terzija et al., "Wide-area monitoring, protection, and control of future electric power networks," *Proceedings of the IEEE*, vol. 99, no. 1, pp. 80-93, 2010.
- [20] D. B. Rathnayake et al., "Grid forming inverter modeling, control, and applications," *IEEE Access*, 2021.
- [21] M. C. Chandorkar, D. M. Divan, and R. Adapa, "Control of parallel connected inverters in standalone AC supply systems," *IEEE transactions on industry applications*, vol. 29, no. 1, pp. 136-143, 1993.
- [22] J. M. Guerrero, L. G. De Vicuna, J. Matas, M. Castilla, and J. Miret, "A wireless controller to enhance dynamic performance of parallel inverters in distributed generation systems," *IEEE Transactions on power electronics*, vol. 19, no. 5, pp. 1205-1213, 2004.
- [23] L. Zhang, L. Harnefors, and H.-P. Nee, "Power-synchronization control of grid-connected voltage-source converters," *IEEE Transactions on Power systems*, vol. 25, no. 2, pp. 809-820, 2010.
- [24] M. Chen, D. Zhou, and F. Blaabjerg, "Modelling, implementation, and assessment of virtual synchronous generator in power systems," *Journal of Modern Power Systems and Clean Energy*, vol. 8, no. 3, pp. 399-411, 2020.
- [25] J. Driesen and K. Visscher, "Virtual synchronous generators," in 2008 IEEE power and energy society general meeting-conversion and delivery of electrical energy in the 21st century, 2008: IEEE, pp. 1-3.



- [26] J. Liu, Y. Miura, and T. Ise, "Comparison of dynamic characteristics between virtual synchronous generator and droop control in inverter-based distributed generators," *IEEE Transactions on Power Electronics*, vol. 31, no. 5, pp. 3600-3611, 2015
- [27] M. E. Meral and D. Çelík, "A comprehensive survey on control strategies of distributed generation power systems under normal and abnormal conditions," *Annual Reviews in control*, vol. 47, pp. 112-132, 2019.
- [28] K. V. Kkuni, S. Mohan, G. Yang, and W. Xu, "Comparative assessment of typical controlrealizations of grid forming converters based ontheir voltage source behaviour," arXiv preprint arXiv:2106.10048, 2021.
- [29] X. Du, Y. Zhang, Q. Li, Y. Xiong, X. Yu, and X. Zhang, "New theory of extended coherency for power system based on method of coherency in differential geometry," in 2011 Asia-Pacific Power and Energy Engineering Conference, 2011: IEEE, pp. 1-6.
- [30] B. B. Johnson, V. Purba, S. Jafarpour, F. Bullo, and S. Dhople, "Reduced-Order Structure-Preserving Model for Parallel-Connected Three-Phase Grid-Tied Inverters," National Renewable Energy Lab.(NREL), Golden, CO (United States), 2017.
- [31] Y. Du, X. Lu, and D. Zhao, "Model Reduction for Inverter-Dominated Networked Microgrids with Grid-Forming Inverters," in IECON 2021–47th Annual Conference of the IEEE Industrial Electronics Society, 2021: IEEE, pp. 1-6.
- [32] P. J. Hart, R. H. Lasseter, and T. M. Jahns, "Coherency identification and aggregation in grid-forming droop-controlled inverter networks," *IEEE Transactions on Industry Applications*, vol. 55, no. 3, pp. 2219-2231, 2019.
- [33] Requirements for the Connection of Micro Generators in Parallel With

Public Low-Voltage Distribution Networks,, 2008. [Online]. Available: https://standards.iteh.ai/catalog/standards/clc/e5472dcd-5831-4f6d-b92a-1069c92911fa/en-50438-2007



Fulbright Grantee 2019.

Muhammad F. Umar (S'18) received the B.Sc. degree in Electrical engineering from Lahore University of Management Sciences, Pakistan, in 2014. He has done Masters in Electrical Power Engineering from U.S. Pakistan Center for Advanced Studies in Energy, National University of Sciences and Technology, Pakistan in 2018. Currently, he is pursuing the Ph.D. degree in Electrical and Computer Engineering Department at University of Illinois at Chicago, USA. He is



Mohsen Hosseinzadehtaher (S'18) received his M.Sc. degree in electrical engineering from Amirkabir University of Technology, Tehran, Iran, in 2014. From 2018 to 2020, he was a Ph.D. student in Electrical and Computer Engineering Department at Kansas State University, Manhattan, USA. Since 2020, he is pursuing the Ph.D. degree in Electrical and Computer Engineering Department at University of Illinois at Chicago, USA. Mr. Hosseinzadehtaher

received the best paper award in the 2nd IEEE SGRE conference in 2019. He is the co-recipient of the "2019 IEEE Foundation Industry Application Society Myron-Zucker Grant".



Mohammad B. Shadmand (M'15-SM'20) received the Ph.D. degree in electrical engineering from Texas A&M University, College Station, TX, USA, in 2015. From 2015 to 2016, he was an Instructor with the Department of Electrical and Computer Engineering, Texas A&M University. From 2016 to 2017, he was a Research Engineer with the Renewable Energy and Advanced Power Electronics Research Laboratory, College Station, TX, USA. From 2017 to 2020, he was an

Assistant Professor with the Department of Electrical and Computer Engineering, Kansas State University, Manhattan, KS, USA. Since 2020, he is an Assistant Professor with the University of Illinois Chicago, IL, USA. He has published more than 100 journal and conference papers. His current research interests include distributed self-learning control schemes, advanced model predictive control, grid-following and grid-forming inverters, and intrusion detection system for power electronics dominated grids.

Dr. Shadmand was awarded Michelle Munson Serban Simu Keystone Research Scholar, Kansas State University in 2017. He was awarded the 2019 IEEE Myron Zucker Faculty-Student Research Grant. He has awarded multiple best paper awards at different IEEE conferences. He is the General Co-Chair of 50th Annual Conference of the IEEE Industrial Electronics Society (IECON 2024), Chicago, IL. He has served as Technical Program Co-Chair of the 2019 and 2022 IEEE Smart Grid & Renewable Energy Conference. He serves as Associate Editor of IEEE Transactions on Industrial Electronics, IEEE Transactions on Industry Application, and IET Renewable Power Generation.